# Graphene coating on silicon anodes enabled by thermal surface modification for high-energy lithium-ion batteries

Sang Cheol Kim, William Huang, Zewen Zhang, Jiangyan Wang, Yongseok Kim, You Kyeong Jeong, Solomon T. Oyakhire, Yufei Yang, and Yi Cui*

Silicon is a high-energy density anode material for lithium-ion batteries, but it possesses shortcomings such as poor electronic conductivity, interfacial instability and mechanical fracturing that hinder its battery cycling. Carbon coating has been an important strategy for stabilizing silicon anodes, but the effects of the silicon surface properties on carbon coating morphology and the consequent silicon cycling stability have not been clearly elucidated. Herein, we find that thermal oxidation of the silicon anodes followed by chemical vapor deposition of carbonaceous precursors leads to a well-ordered graphene coating, whereas disordered graphite coating is formed on the native silicon surface. Graphene-coated silicon exhibits superior cycling performance, retaining a discharge capacity of ~1300 mAh $g^{-1}$ after 300 cycles, whereas the disordered graphite-coated silicon suffers continuous degradation, retaining only ~600 mAh $g^{-1}$ after 300 cycles. Cryogenic electron microscopy reveals the mechanism behind the difference in cycling stabilities; graphene coated silicon is able to withstand the large mechanical strains induced during extended cycling, whereas disordered graphite coating is ruptured, exposing silicon surfaces to the electrolyte, leading to extensive buildup of SEI and poor cycling performance. Characterization of the silicon surface reveals that thermal treatment yields an oxygen-rich surface layer, which is hypothesized to play a decisive role in dictating the carbon coating. This work highlights the effect of silicon surface properties on carbon coating microstructure, and presents thermal treatment as a facile avenue to attain graphene coating on silicon anodes.

## Impact statement

Lithium-ion batteries have become an indispensable element of modern society, powering our mobile devices, electric vehicles, and the grid. For longer-ranged vehicles and longer-running devices, higher-energy density batteries are in demand. Silicon is a promising next-generation anode material, as it offers a capacity of 3570 mAh/g, 10 times that of the current state-of-the-art graphite anode material. However, the adoption of Si anodes is hindered by mechanical fracturing due to volume expansion, poor electrical conductivity, and interfacial instability in contact with the electrolyte. Carbon coating on Si particles plays an integral role in improving these features. The quality of carbon has a critical impact on the performance of the coating: Graphene, compared to disordered carbon, has been suggested to provide superior electrical conductivity, interphase stability, and mechanical integrity. This study deploys cryogenic electron microscopy to reveal the mechanism behind the improved electrochemical performance of graphene-coated silicon.

## Introduction

Silicon (Si) is a promising anode material for next generation Li-ion batteries. It offers a capacity of 3570 mAh $g^{-1}$, 10 times that of the state-of-the-art graphite anode material.[1,2] Because of its outstanding energy density, silicon has attracted extensive attention for the past couple of decades. However, its wide implementation

Sang Cheol Kim, Department of Materials Science and Engineering, Stanford University, USA
William Huang, Department of Materials Science and Engineering, Stanford University, USA
Zewen Zhang, Department of Materials Science and Engineering, Stanford University, USA
Jiangyan Wang, Department of Materials Science and Engineering, Stanford University, USA
Yongseok Kim, Department of Materials Science and Engineering, Stanford University, USA; R&D Center, Samsung SDI, Republic of Korea;
You Kyeong Jeong, Department of Materials Science and Engineering, Stanford University, USA
Solomon T. Oyakhire, Department of Chemical Engineering, Stanford University, USA
Yufei Yang, Department of Materials Science and Engineering, Stanford University, USA
Yi Cui, Department of Materials Science and Engineering, Stanford University, USA; Stanford Institute for Materials and Energy Sciences, SLAC National Accelerator Laboratory, USA; yicui@stanford.edu
*Corresponding author
doi:10.1557/s43577-021-00191-4

in commercial Li-ion batteries has been hindered by its poor mechanical integrity and interphase stability during cycling, as well as its poor electrical conductivity.[1–3] Alongside nanostructuring of silicon anodes, which has been successful for suppressing mechanical fracturing and interphase stability,[4–6] carbon coating has been a widely deployed strategy to improve electronic conductivity, stabilize the interphase, and provide mechanical support.[7–9]

Although carbon coatings provide valuable properties to silicon anodes, not all coatings have the same effect. First, the coating needs to be conformal and uniform. Conformal coatings will protect the silicon surface from exposure to the electrolyte, and coating uniformity is important to prevent Li-ion flux heterogeneities, which may lead to local stress buildup and accelerated degradation.[10] In this aspect, chemical vapor deposition (CVD) is one of the most promising techniques for carbon coating, as it ensures the synthesis of a high quality coating with uniform thickness.[10] CVD is also a scalable process, as it is widely deployed at the industrial scale.[11,12] Second, the atomic arrangement of carbon atoms has a profound impact on battery performance. Highly crystalline graphitic carbon coatings, compared to their amorphous counterparts, have been shown to provide more robust mechanical support, and superior electrical conductivity, which in turn affect the long-term cyclability and the kinetics of the battery.[13] Also, defect sites in amorphous carbon can lead to trapping of Li ions, having a detrimental effect on the initial Coulombic efficiency of the battery.[6] A recent study by Nava et al. highlights the impact of degree of graphitization on battery performance: graphitic carbon coating showed superior cyclability and battery kinetics.[12]

To attain graphene or highly graphitic coatings on silicon anodes, several strategies have been explored.[11,12,14] However, surface modification of Si anodes as a strategy to modulate carbon deposition has not been explored extensively. Because CVD carbon growth is often a surface-controlled process, as is the case on Cu,[15] the surface atop which CVD-derived carbon is grown is likely to have a significant impact on the structure and morphology of carbon. In addition, understanding the relationship between silicon surface properties and carbon coating is critical. Many Si anode synthesis routes exist, including Si synthesis through CVD,[4,9,16] porous micro-Si through acid etching,[17,18] solvothermal synthesis[19] and rapid thermal processing,[20] and each route produces a completely different silicon surface. For example, HF etching produces a relatively oxidation-resistant surface through hydrogen and fluorine termination,[21,22] whereas solvothermal synthesis creates a thick oxide surface layer.[19] Therefore, it is crucial to understand how the properties of silicon surfaces affect subsequent carbon coating.

In this work, we study the effects of silicon surface modification on the structure of carbon coated atop silicon, then extend our insights toward the design of high performing lithium-ion batteries. We synthesized two different silicon surfaces, an oxygen-poor surface and an oxygen-rich surface, and CVD of carbon atop both silicon surfaces results in the formation of highly disordered and ordered carbon coatings, respectively. Compared with the disordered carbon coated on native state silicon, the ordered carbon (graphene) coated on silicon exhibits improved cycle life. The origin of the difference is revealed by cryogenic transmission electron microscopy (cryo-TEM); graphene coating provides a robust mechanical support that maintains its form during repeated lithiation and delithiation, suppressing silicon fracture and preventing excessive solid electrolyte interphase (SEI) formation. In contrast, the disordered graphite coating disintegrates after cycling, exposing the silicon interface to electrolyte, leading to uncontrolled SEI formation. In addition to revealing the benefits of silicon surfaces for the structure of interfacial carbon coatings, we demonstrate the tunability of our approach. The thickness of the graphene coating layer can be easily controlled with deposition time, enabling the precise control of carbon content for silicon-carbon composite anodes.

## Carbon coating fabrication and characterization

Our synthesis process is summarized in **Figure 1**a. It begins with silicon nanoparticles of 100 nm in diameter. Silicon particles are etched with hydrofluoric acid (HF) to obtain pristine silicon particles without oxide layers. Subsequently, the silicon nanoparticles are subjected to different surface oxide formation processes. The first process involves exposure to ambience to form native oxides (Nat-Si) and the other involves thermal treatment at 850°C for 30 min in air (Th-Si). The temperature and duration of the thermal treatment was optimized to ensure a thin dense oxide layer. Carbon was deposited onto the two types of silicon particles (Si and Th-Si) using low pressure chemical vapor deposition (LPCVD) at 900°C for 30 min. Our process was conducted in a tube furnace using hexane as the carbon source and argon as the carrier gas (Supplementary Material **Figure S1**).

Carbon layers deposited on the two types of silicon particles exhibit strikingly different structure and crystallinity. Figure 1b–c shows the high-resolution transmission electron microscope (HR-TEM) images of carbon coated on silicon without thermal treatment (Nat-Si@C) and silicon with thermal treatment (Th-Si@C), respectively. Figure 1b shows disordered graphite coated on Nat-Si, where graphitic crystalline domains are fragmented. In contrast, as shown in Figure 1c, graphene was coated on Th-Si, where the crystalline graphitic domains extend over the silicon nanoparticle, providing a conformal coating. The different crystallinities of the coatings are further supported by Raman spectra, as shown in the insets of Figure 1b and c. For Th-Si@C, the G band and D band have similar intensities, with I(D)/I(G) of 1.07. However, for Si@C, the G band is more pronounced than the D band (I(D)/I(G) of 1.20), suggesting a more disordered nanocrystalline graphite for Si@C.[23] In addition, we observe the presence of 2D band—a fingerprint for graphene—in Th-Si@C, while it is nearly absent in Si@C. From HR-TEM and Raman spectroscopy, it is evident that thermal

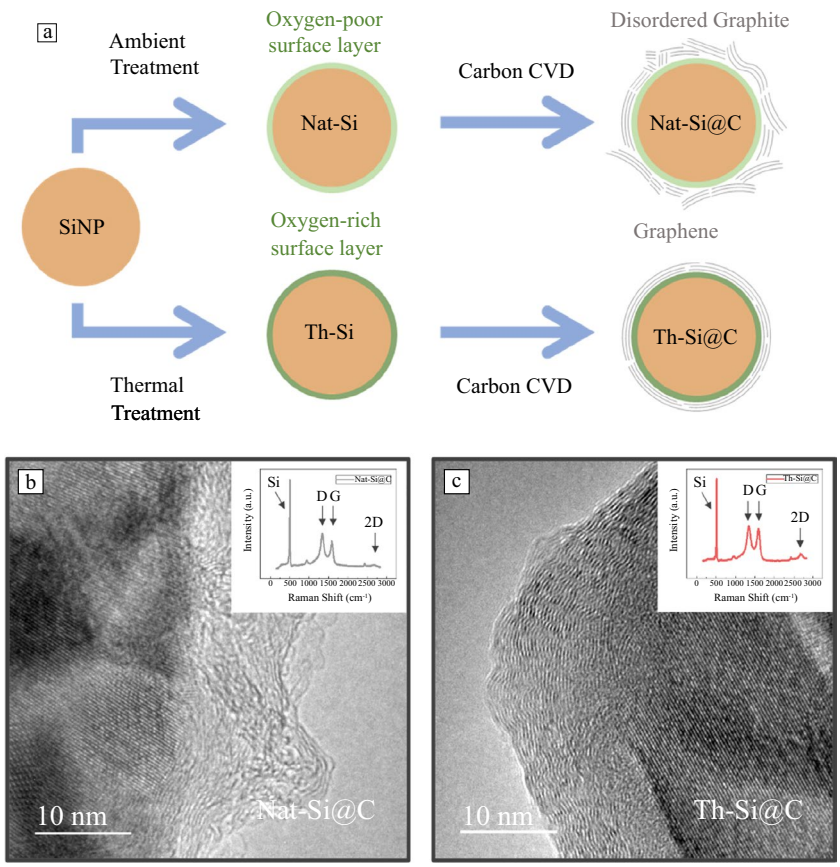


**Figure 1.** Carbon coating fabrication and characterization. (a) SiNP undergo two different treatments, thermal treatment resulting in Th-Si and ambient treatment resulting in Nat-Si. When carbon is coated via CVD on the two silicon materials, (a) graphene coating forms on Th-Si whereas disordered graphitic coating forms on Nat-Si. (b) HR-TEM image and Raman spectrum of Nat-Si@C show a disordered graphitic carbon coating. (c) HR-TEM image and Raman spectrum of Th-Si@C show graphene coating.

treatment of silicon in air yields a much more crystalline carbon structure.

## Cycling performance and cryogenic electron microscopy characterization

A major challenge for the silicon anode is its long-term cycling performance, often plagued by mechanical fracturing and unstable interphase. We investigate the effects of carbon coating crystallinity on the Si anode electrochemical performance (**Figure 2**a and **Figure S3**). Figure 2a shows that thermally treated silicon (Th-Si@C) retains 1300 mAh $g^{-1}$, 75.7% of its initial capacity, after up to 300 cycles. On the other hand, Nat-Si@C continuously loses capacity, retaining only about 600 mAh $g^{-1}$ after 300 cycles, which amounts to only 35.7% of its initial capacity. In addition, Th-Si@C shows a high average Coulombic efficiency of 99.7%, whereas Nat-Si@C shows a lower value of 99.1 percent.

To investigate the nanoscopic origin of this difference, we used electron microscopy to study the electrode and particle morphologies. Figure 2b–c shows the microscopic view of the electrode, imaged using the scanning electron microscope (SEM). It shows that Nat-Si@C has extensive cracking of the electrodes, but Th-Si@C has much less cracking. To further study the particle morphologies and the SEI after cycling, cryogenic transmission electron microscopy (cryo-TEM) was deployed. Because SEI is prone to beam damage, it is difficult to retain its original state using conventional electron microscopy. Cryo-TEM is an effective tool that overcomes these challenges, as the cryogenic temperature preserves the SEI in its pristine state and minimizes damage from the electron beam.[24] Figure 2d and **Figure S4** show the HR-TEM images of cycled Nat-Si@C, and Figure 2e and **Figure S5** show that of cycled Th-Si@C. Striking differences can be seen, where Nat-Si@C particle and coating are fractured, exposing silicon surfaces to the electrolyte, while Th-Si@C retains its spherical shape. Figure 2f–g show magnified images that illustrate the interphases. Th-Si@C has a thin uniform amorphous SEI of ~3 nm, but Nat-Si@C has SEI of nonuniform thickness, ranging up to tens of nanometers. The structural integrity of the particles directly affects the cycling performance. The rupturing of Nat-Si@C not only leads to additional surface for passivation, but also leads to a less stable interphase that forms on silicon.[3] This results in an uncontrolled SEI growth, with SEI thicknesses ranging up to tens of nanometers (Figure 2d) and ultimately a lower Coulombic efficiency (Figure 2a). In contrast, Th-Si@C retains its structural integrity, preventing further surface exposure and excessive SEI growth. In addition, whereas graphene coatings effectively suppress the fracturing of silicon particles, disordered graphite coatings fail to do so. Nat-Si@C particles crack after cycling, which could lead to loss of electrical contact and capacity degradation.

The marked differences in silicon morphology and SEI of the two cycled electrodes can be attributed to the mechanical properties of the coatings. Li et al. demonstrated that graphene

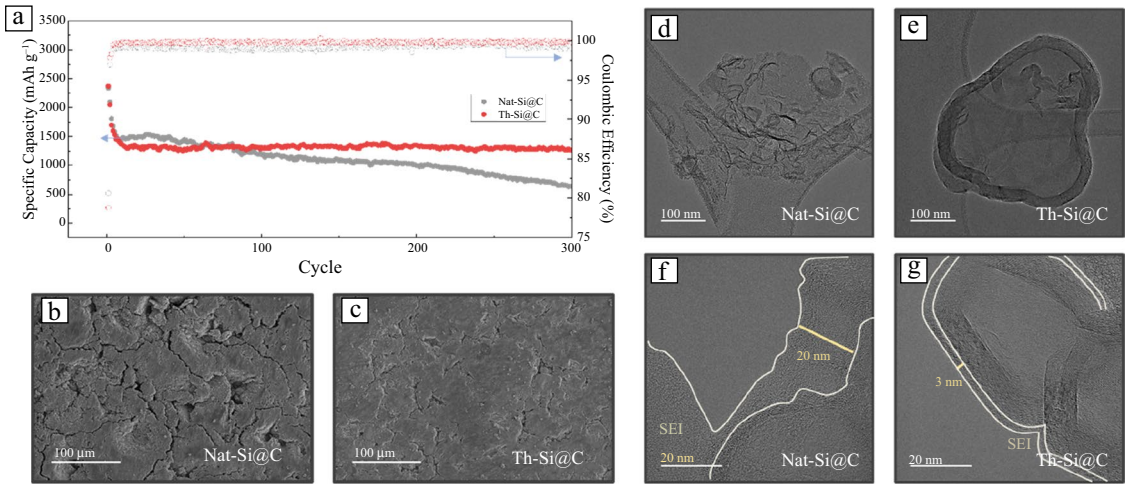


**Figure 2.** Cycling performance and electron microscopy characterization. (a) Electrochemical cycling of silicon half-cells. Th-Si@C shows a stable capacity up to 300 cycles, but Nat-Si@C shows a continuous decay of capacity. Open circle markers represent CE while closed circle markers represent specific capacity. (b) SEM image of cycled Nat-Si@C electrode shows deep crack formation. (c) SEM image of cycled Th-Si@C shows less severe crack formation. (d) and (f) Cryo-TEM images of cycled Nat-Si@C show particle cracking and extensive SEI buildup. (e) and (g) Cryo-TEM images of cycled Th-Si@C show retained particle structure and thin SEI.

coating has much greater resistance to fracture under mechanical stress than amorphous carbon using *in situ* TEM.[13] It has also been proposed that sliding mechanism enables graphene to accommodate volume expansion of silicon during lithiation and retain its structural integrity.[14,25] We hypothesize that similar mechanisms are acting to safeguard graphene coatings, whereas disordered graphite coatings are mechanically weaker, and cannot accommodate volume change through sliding mechanism.[13,14] It has also been reported that lithiation increases graphene interlayer sliding friction by 7 times.[26] It can be reasoned that during anode lithiation, silicon—which has a higher lithiation potential than graphite—will react first, while the unlithiated graphene retains its ease of sliding, thereby accommodating the volume change of silicon. Subsequent graphene lithiation renders the coating to be mechanically strong, further preventing fracture of the coating as well as the silicon particles. During delithiation, lithium is extracted from graphene, enabling sliding and to accommodate the subsequent silicon contraction. We postulate that the dynamic mechanical properties of the graphene coating lead to superior structural integrity and cycling stability of Th-Si@C.

## Silicon surface characterization

Because chemical vapor deposition (CVD) of graphene is often a surface-controlled process, as is in the case on Cu,[15] characterizing the surface layer is essential for gaining insights into the mechanism behind the different crystallinities of carbon coatings. The morphologies of the silicon surface layers are imaged using HR-TEM (**Figure 3**a, b and **Figure S6**). The oxide layer can be distinguished from the bulk silicon through differences in crystallinity; bulk silicon is crystalline, with its lattice structure is clearly shown, while $SiO_x$ is amorphous. It is shown that the thicknesses of the oxide layers are comparable: both Th-Si and Si have amorphous oxide layer thicknesses of ~2 nm. Contrary to the similar oxide thicknesses, x-ray photoelectron spectroscopy (XPS) reveals clearly different chemical compositions of the two layers (Figure 3c–d). The survey spectrum shows a less pronounced O 1*s* peak relative to the Si 2*p* peak, signifying a smaller oxygen content. A more striking comparison can be seen for the Si 2*p* spectrum. The oxidation states of the silicon in Th-Si is primarily $Si^{4+}$, signifying silicon oxidation to $SiO_2$, while silicon in Nat-Si exists primarily as $Si^0$. In addition, although oxidized silicon is primarily $Si^{4+}$, it can also be seen that intermediate oxidation states between $Si^{1+}$ to $Si^{3+}$ coexist, signifying incomplete oxidation of Si in the oxide layers. This clearly portrays that although the relative thicknesses of the amorphous oxide layers seem similar, the composition of the oxide layer is starkly different, with Th-Si showing higher extent of oxidation.

There are two potential mechanisms for how the oxygen-rich surface layer promotes graphene deposition. First possibility is that oxygen acts to remove hydrogen radicals, promoting $sp^2$ carbon over $sp^3$ carbon.[27] Hydrogen radicals are generated during the decomposition of hydrocarbon precursors. These radicals can compete with carbon species in the growth process, and lead to formation of $sp^3$ carbon, which introduce defect sites that lower the crystallinity of graphene.[27] Therefore, if oxygen can react with H radicals and remove them, graphene growth will be promoted. Using such principles, Son

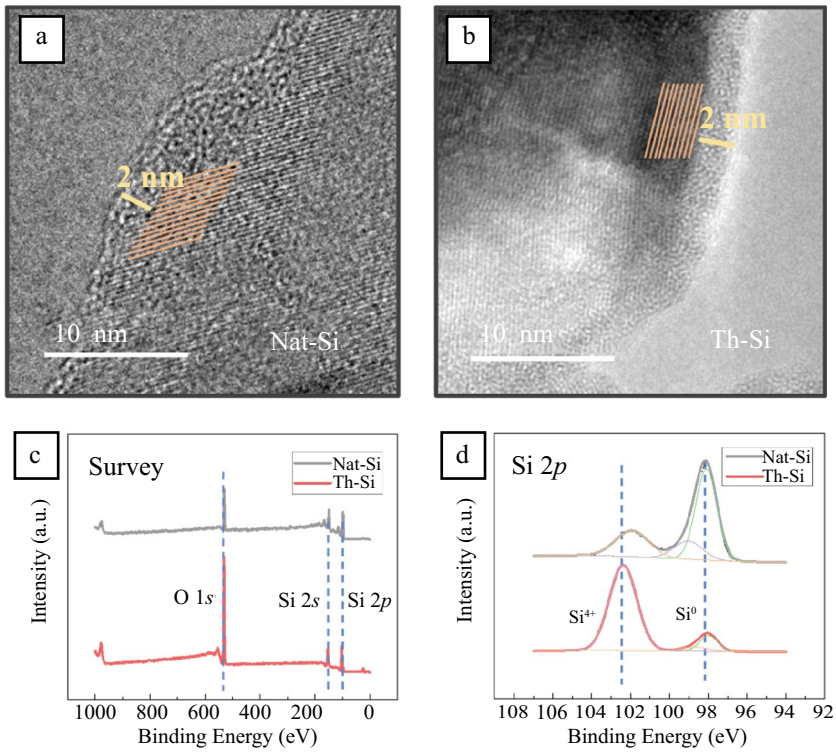


**Figure 3.** Silicon surface characterization. (a) and (b) HR-TEM images of Nat-Si and Th-Si, respectively. Both show a similar thickness of amorphous oxide layer. (c) XPS survey spectra show that oxygen peak intensity is relatively strong for Th-Si. (d) XPS Si 2*p* spectra show that Th-Si has greater oxidized silicon composition, signifying higher oxygen content.

et al. showed that graphene can be grown on silicon particles through the introduction of mild oxidants during CVD.[14] The same group reported in a different investigation that $SiO_2$ particles shrunk during CVD of carbon, suggesting that oxygen in $SiO_2$ was consumed.[28] However, in our study we did not observe compositional and morphological changes in the oxide layers after carbon deposition, which could be a result of different reaction temperature and the different substrate. **Figure S7** shows the XPS of Th-Si@C, which reveals that the oxidation states of silicon are unchanged after CVD coating. Also, as can be seen in **Figure S8** the amorphous oxide layer after coating remains to be about 2–3 nm, which is similar to the oxide before carbon deposition.

Our analysis points in the direction of another possible mechanism, in which surface oxygen assists adsorption of carbon species, aiding conformal growth. Liu et al. conducted density functional theory (DFT) calculations that revealed favorable adsorption energy of carbonaceous precursors for $SiO_x$ (−0.24 eV) compared with Si (0.21 eV),[29] which aids the conformal coverage of adsorbed carbon precursors on oxygen-rich surfaces, allowing for a more ordered growth. Chen et al. also suggest a surface-controlled mechanism of graphene deposition on glass, where the carbon atoms bind to the surface oxygen, followed by nucleation and growth.[15] Dense oxygen sites available for carbon adsorption may enable a more uniform and conformal growth of graphene, whereas sparse oxygen atoms may provide insufficient sites for binding and growth, leading to a more disordered graphite structure.

## Tunability of the graphene coating

As carbon coatings play an integral role in battery performance, tunability of coating properties is also important; the ability to modulate the coating for battery performance optimization offers a potent engineering tool. In particular, tuning the carbon content, coating thickness and surface area are critical parameters that are directly related to battery performance metrics; increasing carbon content and coating thickness compromises anode capacity but improves cycling stability,[25] while decreasing specific surface area boosts initial Coulombic efficiency.[30] Therefore, it is important to find an optimal point for these properties. In addition, the coating process must be applicable to different silicon substrates for widespread adoption.

Here we apply the graphene coating method on porous microsilicon particles and tune the properties by varying the coating time duration. Porous microsilicon particles are promising anode materials for practical applications, as they have nanoporous structures that accommodate volume expansion, as well as reduced surface area compared with silicon nanoparticles.[17] **Figures 4**a–c shows the graphitic coatings on porous silicon microparticles for various deposition durations ranging from 90 to 270 min. First of all, it is evident that our coating process is compatible with porous microparticles as well, conformally coating the porous surfaces with highly graphitic layers (Figure 4a–c). Figure 4d–f shows the dependence of carbon content, coating thickness, and specific surface area on coating duration. We see that carbon content increases with coating duration, from 17% at 90 min to almost 50% after 270 min. Coating thickness also increases from ~7 nm after 90 min to ~36 nm after 270 min. Carbon content and coating thickness increase in a near linear fashion with coating duration, enabling facile and precise control. Specific surface area, on the other hand, decreases with increased coating times, from 55 $m^2\ g^{-1}$ at 90 min to less than 10 $m^2\ g^{-1}$ at 270 min. As shown in **Figure S8**, as coating duration increases, the pores of the microparticles become filled with

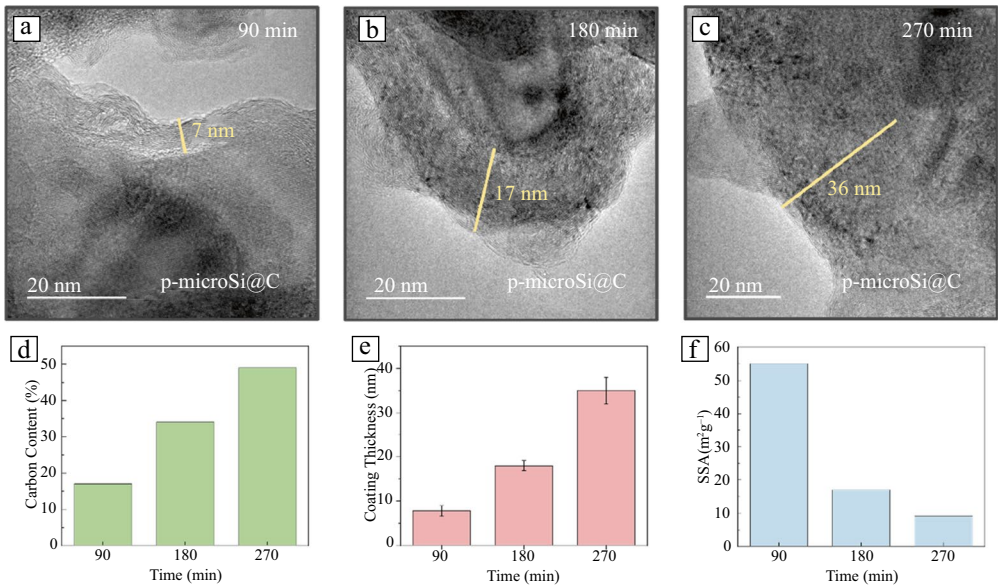


**Figure 4.** Tunability of graphene coating. (a–c) HR-TEM images of carbon coating on porous microSi with different deposition durations, ranging from 90 to 270 min. (d) Carbon content increases with coating duration. (e) Coating thickness increases with coating duration. (f) Specific surface area decreases with coating duration.

carbon, decreasing the specific surface area. After 270 min of coating, it essentially yields a silicon-graphite composite, allowing for facile synthesis of a composite anode material with low surface area. We demonstrate that our coating method can be applied to porous microsilicon particles to produce conformal and highly graphitic coatings. We also demonstrate how carbon content, coating thickness, and surface area can be controlled by using CVD duration as a turning knob, enabling the fabrication of carbon coatings that can be suited to fit the needs of different battery systems.

## Conclusion

In this article, we study the effects of silicon surface properties on carbon coating via chemical vapor deposition. We find that thermal oxidation of silicon particles, which introduces an oxygen-rich surface layer atop silicon, supports the CVD growth of a graphene coating, whereas an oxygen-poor native oxide leads to a disordered carbon coating. Graphene coated silicon retains 1300 mAh $g^{-1}$ of capacity after 300 cycles, whereas disordered carbon coated silicon only retains 600 mAh $g^{-1}$. Cryo-TEM reveals that graphene coating preserves the structural integrity of silicon particles after cycling, whereas disordered graphite coating ruptures and fails to suppress the mechanical fracturing of silicon particles. This leads to excessive formation of SEI as well as potential loss of particle contact. Based on the understanding of the relationship between surface oxides and carbon coating, we present surface tuning as a strategy for the facile synthesis of graphene coating and explore its application in porous microsilicon with high tunability. We expect that this study sheds light on the relationship between silicon surface properties and carbon coating, and also introduces a novel coating synthesis methodology for high-performance silicon anodes.

## Methods

### *Carbon coating of silicon nanoparticles and porous microsilicon*

Silicon nanoparticles of approximately 100 nm diameter were used as received (MTI). All silicon samples were etched with hydrofluoric acid (10% in 1:3 water/isopropanol v/v solution) for 30 min and rinsed to remove existing oxides to eliminate any variability in the surface. Thermally treated silicon (Th-Si) was then heated in air in 850°C for 30 min in a tube furnace. Native state silicon (Nat-Si) was stored in ambient atmosphere for two months before use. Each of the pretreated silicon nanoparticles were coated with carbon using low-pressure chemical vapor deposition (LPCVD). N-hexane (Sigma-Aldrich) was used as the carbon precursor and argon (Praxair) was used as the carrier gas. A vacuum pump was used to reduce the deposition pressure and induce vaporization of hexane, and a pressure gauge was used to measure the downstream pressure. Before coating all samples were purged with Ar at low pressure (550 mtorr) for 30 min, and the reaction chamber was heated to 900°C at 15°C $min^{-1}$. Then hexane was flowed into the reaction chamber, and its flow was controlled to meet a pressure of 850 mtorr and carbon was deposited for 30 min. Porous microsilicon was synthesized in a methodology as described by Wang et al.[31] Carbon coating was conducted in the same manner, with varying time durations.

### *Electrochemical performance testing*

Silicon electrodes were fabricated using a slurry coating method. Nat-Si@C and Th-Si@C particles were mixed with poly(vinylidene fluoride) (PVDF, Kynar HSV 900) binder and carbon black (Timcal Super-C65) in 8:1:1 mass ratio in *N*-methyl-2-pyrrolidone solvent to form a slurry. The slurry

was casted on 10 μm copper foil and the electrode was dried at 60°C in vacuum oven for 24 h then calendered. The electrodes were cut into 1 $cm^2$ disks with mass loading ~0.6 mg $cm^{-2}$. In an argon-filled glovebox, the silicon electrodes were assembled into Li | Si type 2032 coin cell batteries. Each coin cell used Li foil (Alfa Aesar) as counter electrode, separator (Celgard 2325) and 70 μL of electrolyte. The electrolyte composition was 1 M $LiPF_6$ in ethylene carbonate (EC) – diethyl carbonate (DEC) (BASF LP40) added with 10% (v/v) fluoroethylene carbonate (FEC) as additive. Coin cell cycling was done using cyclers (Land Instruments). The cell underwent 2 cycles of formation at C/20 between 0.01 V and 1 V, and were cycled at C/2 for subsequent cycles.

### *Materials characterization*

The two silicon samples (Nat-Si@C and Th-Si@C) were each characterized. High-resolution transmission electron microscopy (HR-TEM) images were taken with an FEI Tecnai and an FEI Titan 80–300. Coating thickness was measured using HR-TEM images, using an average of 10 samples. Surface area was measured using a Quantachrome Autoflow BET+ using Brunauer–Emmett–Teller (BET) theory calculations. X-ray photoelectron spectroscopy (XPS) characterization of the coated and uncoated samples was conducted using PHI VersaProbe 1. Raman spectroscopy was conducted using Horiba Xplora+. Carbon content was measured using a TG/DTA instrument (Netzsch STA 449). Sample was heated (5°C/min) in a 20% $O_2$ 80% Argon atmosphere, and the mass loss, which is attributed to carbon content, was measured.

### *Electron microscopy characterization of cycled electrodes*

The two silicon samples were cycled at C/2 for 100 cycles. After full discharge, the cycled electrodes were opened in an argon-filled glovebox, rinsed with diethyl carbonate. For scanning electron microscopy (SEM) the electrode was directly transferred into a SEM holder and imaged using an FEI Magellan 400 XHR scanning electron microscope. For cryo-transmission electron microscopy (cryo-TEM) the electrode particles were transferred onto copper grids with lacey carbon in an argon-filled glovebox. The grids were transferred out of the glovebox in a argon-filled sealed container. While being submerged in liquid nitrogen, the grid was transferred into a specialized holder where air exposure is prevented and the temperature was maintained at −178°C. Cryo-TEM was conducted using an FEI Titan 80–300, operated at an voltage of 300 kV and energy resolution of 1 eV.

## Acknowledgments

Part of this work was performed at the Stanford Nano Shared Facilities (SNSF), supported by the National Science Foundation under award ECCS-2026822. The HR-TEM images were taken with a K3 IS camera and support is courtesy of Gatan Inc. Z.Z. acknowledges the support of Stanford Interdisciplinary Graduate Fellowship. S.T.O. acknowledges support from the Knight Hennessy scholarship for graduate studies at Stanford University.

## Author Contributions

S.C.K. and Y.C. conceived and designed the experiments. S.C.K. conducted coating fabrication, materials characterization, and electrochemical performance testing. W.H. conducted room temperature TEM experiments. Z.Z. conducted cryo-EM experiments. J.W. prepared porous microsilicon particles. S.C.K. and Y.C. co-wrote the paper. All authors discussed the results and commented on the manuscript.

## Conflict of interest

The authors declare no competing financial interests.

## Supplementary information

The online version of this article contains supplementary material available at https://doi.org/10.1557/s43577-021-00191-4.

## References

1. Y. Liu, G. Zhou, K. Liu, Y. Cui, *Acc. Chem. Res.* **50**, 2895 (2017)
2. M.T. McDowell, S.W. Lee, W.D. Nix, Y. Cui, *Adv. Mater.* **25**, 4966 (2013)
3. W. Huang et al., *Matter* **1**, 1232 (2019)
4. C.K. Chan et al., *Nat. Nanotechnol.* **3**, 31 (2008)
5. Y. Yao et al., *Nano Lett.* **11**, 2949 (2011)
6. N. Liu et al., *Nat. Nanotechnol.* **9**, 187 (2014)
7. S. Chen, L. Shen, P.A. van Aken, J. Maier, Y. Yu, *Adv. Mater.* **29**, 1605650 (2017)
8. J. Wang et al., *Nano Energy* **61**, 404 (2019)
9. J. Wang et al., *Nano Lett.* **18**, 7060 (2018)
10. H. Li, H. Zhou, *Chem. Commun.* **48**, 1201 (2012)
11. J. Yu et al., *Ind. Eng. Chem. Res.* **53**, 12697 (2014)
12. G. Nava, J. Schwan, M.G. Boebinger, M.T. Mcdowell, L. Mangolini, *Nano Lett.* (2019). https://doi.org/10.1021/acs.nanolett.9b02835
13. Y. Li et al., *Nat. Energy* **1**, 1 (2016)
14. I.H. Son et al., *Nat. Commun.* **6**, 1 (2015)
15. Z. Chen, Y. Qi, X. Chen, Y. Zhang, Z. Liu, *Adv. Mater.* **31**, 1 (2019)
16. M. Ko et al., *Nat. Energy* **1**, 1 (2016)
17. J. Wang et al., *Nano Res.* **13**, 1558 (2020)
18. W. An et al., *Nat. Commun.* **10**, 1 (2019)
19. L. Lin, X. Xu, C. Chu, M.K. Majeed, J. Yang, *Angew. Chem.* **128**, 14269 (2016)
20. H.G. Tan, J.G. Duh, J. Power Sources **335**, 146 (2016)
21. G.S. Higashi, Y.J. Chabal, G.W. Trucks, K. Raghavachari, *Appl. Phys. Lett.* **56**, 656 (1990)
22. B.R. Weinberger, G.G. Peterson, T.C. Eschrich, H.A. Krasinski, *J. Appl. Phys.* **60**, 3232 (1986)
23. A.C. Ferrari, J. Robertson, *Phys. Rev. B* **61**, 14095 (2000)
24. Y. Li et al., *Science (-80)* **358**, 506 (2017)
25. X. Han et al., *ACS Appl. Mater. Interfaces* **12**, 44840 (2020)
26. Z. Pang et al., *Extrem. Mech. Lett.* **35**, 100616 (2020)
27. G. Zhang et al., *Proc. Natl. Acad. Sci. U.S.A.* **102**(45), 16141 (2005)
28. I.H. Son et al., *Nat. Commun.* **8**, 1561 (2017)
29. B. Liu et al., *J. Am. Chem. Soc.* **133**, 197 (2011)
30. D. Lin et al., *Energy Environ. Sci.* **8**, 2371 (2015)
31. J. Wang et al., *Nano Res.* **13**, 1558 (2020)